Minimal model of binary fluid convection

Edgar Knobloch
Department of Physics, University of California, Berkeley, California 94720

Daniel R. Moore*
Institute for Naval Oceanography, NSTL, Mississippi 39529
(Received 29 September 1989; revised manuscript received 2 April 1990)

Steady and oscillatory convection in a binary fluid mixture heated from below is considered. Stress-free and fixed temperature and concentration boundary conditions are used at the top and bottom, with periodic boundary conditions in the horizontal. A minimal Galerkin truncation is constructed such that the local branching behavior near both the steady state and Hopf bifurcations is correctly determined. To do this, modes generated through fourth order in perturbation theory must be retained. The properties of the steady states and standing, traveling, and modulated traveling waves in the resulting system are systematically analyzed. Broad agreement with the results of an analysis of a codimension-two bifurcation with O(2) symmetry is found.

I. INTRODUCTION

Convection in a binary fluid mixture exhibits a rich variety of dynamical behavior that has been extensively studied in recent years. At the same time a theory exploiting the presence of an approximate O(2) symmetry has been found to account for some of the observed behavior. A brief review of these developments is given in Ref. 1.

The equations describing two-dimensional convection in a binary fluid mixture of infinite horizontal extent and homogeneous boundary conditions are equivariant under the group E(1) of translations. In addition they are equivariant with respect to reflections in a vertical plane. In the presence of periodic boundary conditions in the horizontal the full symmetry $E(1)\times Z_2$ reduces to the subgroup O(2) of rotations and reflections of a circle. The theory[2-4] points out that owing to the symmetry there are two solution branches which bifurcate simultaneously from the conduction solution at a Hopf bifurcation. One branch, corresponding to standing waves (hereafter SW) arises already in the absence of translation symmetry, i.e., when no horizontal flux boundary conditions are imposed on impenetrable vertical sidewalls. We refer to this as the Z_2-symmetric problem. The second branch, corresponding to traveling waves (hereafter TW), occurs only in the presence of translation symmetry and periodic boundary conditions permitting the *propagation* of disturbances. The theory establishes conditions under which either branch is locally stable, and has been found to be in complete agreement with numerical simulation of thermosolutal convection.[3,5] Likewise, the study of a particular multiple bifurcation, the Takens-Bogdanov (hereafter TB) bifurcation has been successful in accounting for much of the behavior associated with the interaction of the SW branch with the branch of steady overturning convection (the steady-state or SS branch) in Z_2-symmetric thermosolutal convection.[6,7] This analysis has recently been extended to the O(2)-symmetric TB bifurcation,[8] and the question naturally arises as to the extent to which it can be used to understand the dynamics observed in the O(2)-symmetric system.

In the present paper we construct a system of ordinary differential equations describing convection in a binary fluid mixture. We seek a system that is as small as possible so that it can be investigated in some detail without undue expense. We demand, however, that it correctly predicts the local bifurcation behavior of the partial differential equations near both the Hopf and steady-state bifurcations from the conduction solution. The system so constructed is *minimal* in that only those modes which enter into the determination of the directions of branching are retained. Since it is well known that with the boundary conditions we use (stress-free boundaries at top and bottom, and fixed temperature and concentration) the bifurcation to TW is degenerate[9] it is immediately clear that the minimal system must include modes generated through fourth order in perturbation theory. It turns out, however, that not all such modes are required, so that the resulting system consists of a rather modest nine (complex) equations. We discuss here the properties of this system, and compare them with the analysis of the TB bifurcation.[8] We find that the latter provides the correct qualitative description of the dynamics of the model, including secondary branches of modulated waves (hereafter MW), for a wide range of parameter values. The one qualitative difference we have been able to pinpoint is the presence, under appropriate circumstances, of a new type of global bifurcation with which the MW branch terminates. In addition, we find that the interaction of

the traveling waves with a saddle-node bifurcation on the steady-state branch, a prominent feature of the present system, can be understood in terms of a rather simple three-dimensional vector field derived from the normal form for a degenerate TB bifurcation. Owing to the success of a similar procedure in describing the dynamics of the partial differential equations in Z_2-symmetric thermosolutal convection[7] we surmise that the model system provides a similarly good model of the O(2)-symmetric partial differential equations, at least for moderate amplitudes. These conclusions also apply to thermosolutal convection with O(2) symmetry, stress-free boundaries and fixed temperature and concentration at the top and bottom[3,5] since the two problems can be transformed into one another.[10]

This paper is organized as follows. In Sec. II the minimal system is constructed. The results of a systematic numerical exploration of this system are presented in Sec. III. A theoretical analysis of some of these results is described in Sec. IV, and is based on a normal form derived in the Appendix. The conclusions follow in Sec. V.

II. THE MINIMAL SYSTEM

The basic equations describing two-dimensional Boussinesq convection in a binary fluid mixture heated from below can be written in the nondimensional form[4]

$$\frac{1}{\sigma}[\nabla^2\psi_t + J(\psi,\nabla^2\psi)] = R\theta_x + RS\Sigma_x + \nabla^4\psi, \tag{1a}$$

$$\theta_t + J(\psi,\theta) = \psi_x + \nabla^2\theta, \tag{1b}$$

$$\Sigma_t + J(\psi,\Sigma) = \psi_x - \tau\nabla^2\theta + \tau\nabla^2\Sigma. \tag{1c}$$

Here ψ is the stream function, θ and Σ represent departures of the temperature and concentration from the linear profiles present in the absence of the motion, while σ, τ ($\tau < 1$), S, and R denote, respectively, the Prandtl number, the Lewis number, the separation ratio, and the Rayleigh number. These equations are supplemented by stress-free boundary conditions at the top and bottom,

$$\psi = \psi_{zz} = 0 \quad \text{on} \quad z = 0,1. \tag{2a}$$

In addition, we assume that both the temperature and concentration are fixed on the boundaries,

$$\theta = \Sigma = 0 \quad \text{on} \quad z = 0,1. \tag{2b}$$

This choice of boundary conditions has the advantage that only a finite (and small) number of modes enter into the determination of the local branching behavior of the solutions. Consequently the minimal system we construct below has a well-defined regime in which it becomes *exact* . This desirable property is not shared by the model proposed in Ref. 11 for no-mass-flux boundary conditions.

The conduction solution ($\psi = \theta = \Sigma = 0$) loses stability at a Hopf bifurcation when R reaches[12]

$$R_{\text{Hopf}} \equiv \frac{(1+\tau)(1+\sigma)(\tau+\sigma)}{\sigma[1+\sigma(1+S)]}R_0 \tag{3}$$

provided

$$S < S_c \equiv \frac{-\tau^2(1+\sigma)}{\sigma+\tau(1+\tau)(1+\sigma)}, \tag{4}$$

and loses stability at a steady-state bifurcation when R reaches

$$R_{\text{SS}} \equiv \frac{\tau}{\tau+(1+\tau)S}R_0. \tag{5}$$

Here $R_0 \equiv p^3/k^2$, $p \equiv k^2+\pi^2$, is the Rayleigh number for the onset of Rayleigh-Bénard instability with horizontal wave number k in a pure fluid. It is minimized by $k = \pi/\sqrt{2}$, a value of k used for the computations described in Sec. III.

As discussed in the Introduction, the bifurcation at R_{Hopf} gives rise to branches of traveling and standing waves which we may write in the following form. For TW,

$$R = R_{\text{Hopf}} + \varepsilon^2 R_2^{\text{TW}} + \varepsilon^4 R_4^{\text{TW}} + \cdots, \tag{6a}$$

$$c = c_0 + \varepsilon^2 c_2^{\text{TW}} + \varepsilon^4 c_4^{\text{TW}} + \cdots, \tag{6b}$$

and for SW,

$$R = R_{\text{Hopf}} + \varepsilon^2 R_2^{\text{SW}} + \varepsilon^4 R_4^{\text{SW}} + \cdots, \tag{7a}$$

$$\omega = \omega_0 + \varepsilon^2\omega_2^{\text{SW}} + \varepsilon^4\omega_4^{\text{SW}} + \cdots . \tag{7b}$$

Here ε is the amplitude of motion, c is the phase velocity of the TW, while ω is the frequency of the SW. Similarly, the bifurcation at R_{SS} gives rise to a branch of steady overturning convection:

$$R = R_{\text{SS}} + \varepsilon^2 R_2^{\text{SS}} + \varepsilon^4 R_4^{\text{SS}} + \cdots . \tag{8}$$

The coefficients R_2^{TW}, R_2^{SW}, and R_2^{SS} are well known;[4] in particular, $R_2^{\text{TW}} \equiv 0$ (Ref. 9). Consequently, the coefficient R_4^{TW} determines the direction of branching of the TW branch. In Fig. 1(a) we show the line $R_4^{\text{TW}} = 0$ in the (σ,τ) plane for several values of S. The curves are not particularly sensitive to S. We observe that for most choices of σ,τ the TW branch is supercritical ($R_4^{\text{TW}} > 0$). The branch is subcritical ($R_4^{\text{TW}} < 0$) only for rather small Prandtl numbers σ. The direction of branching of the SW branch is determined by R_2^{SW}. We find that when $S = -1$, $R_2^{\text{SW}} \to 0$ as $\sigma \to \infty$, and is positive for finite σ. For $-1 < S < S_c$ it is always positive.[13] The curves $R_4^{\text{TW}} = 0$ and $R_2^{\text{SW}} = 0$ do not intersect for any value of S. Consequently, only two possibilities are likely to arise, (i) $R_4^{\text{TW}} < 0$, $R_2^{\text{SW}} > 0$, and (ii) $R_4^{\text{TW}} > 0$, $R_2^{\text{SW}} > 0$. In the former case theory[3] shows that the TW branch is unstable, while in the latter it is stable. The SW branch is unstable in both cases. A third possibility (iii) $R_4^{\text{TW}} > 0$, $R_2^{\text{SW}} < 0$ occurs for extreme values of S only, as shown in Fig. 1(b) for $S = -2.0$. Note that the transition between regions (ii) and (iii) must occur via a very narrow region in which the

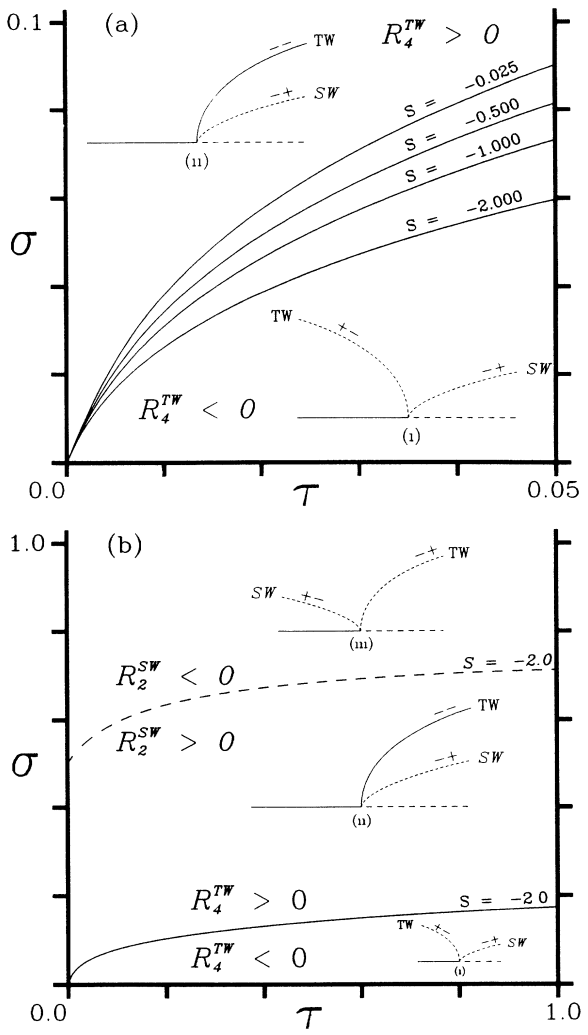

FIG. 1. (a) Lines of $R_4^{\mathrm{TW}} = 0$ in the (τ, σ) plane for various values of the separation parameter S. (b) The lines $R_4^{\mathrm{TW}} = 0$ (solid) and $R_2^{\mathrm{SW}} = 0$ (dashed) on a larger region of the (τ, σ) plane for S =−2.0. Schematic bifurcation diagrams for each of the three regions are drawn as insets. Stability properties with respect to amplitude and phase perturbations are indicated by + (unstable) and − (stable). Region (iii) is present for sufficiently negative values of S only.

SW branch is stable and the TW branch unstable. This region is not indicated in Fig. 1(b).

The bifurcation to steady convection is subcritical if $S < S_{\mathrm{ct}}$ and supercritical if $S > S_{\mathrm{ct}}$, where

$$S_{\mathrm{ct}} \equiv \frac{-\tau^3}{(1+\tau)(1+\tau^2)}. \tag{9}$$

It is easy to check that $S_{\mathrm{ct}} > S_c$ always, so that when the Hopf bifurcation precedes the steady-state bifurcation the SS branch is subcritical and unstable. At the codimension-two point, $R = R_{\mathrm{ct}} \equiv (1+\tau^2)R_0$, $S = S_{\mathrm{ct}}$, the direction of branching is determined by R_4^{SS}. We find that

$$R_4^{\mathrm{SS}} = \frac{2+2\varpi}{1+2\varpi}\frac{R_0}{\tau^2}, \tag{10}$$

where $\varpi \equiv 4\pi^2/p$ $(0 < \varpi < 4)$ is a measure of the wave number of the instability. This result disagrees with that of Ref. 14 but has been checked using CAMAL .[15]

In Table I we list those modes that contribute to the determination of the above coefficients. A number of other modes that are generated at $O(\varepsilon^4)$ do not contribute and are omitted from the table. Among these is another x-independent ψ mode, $\sin 4\pi z$; these modes represent lateral streaming with velocity $u(z) = -\psi_z$. The implication of such an Eulerian mean flow for the transport properties of traveling waves will be explored elsewhere.[16,17] In SW or SS convection the amplitude of these modes vanishes, however, and the mean flow is absent.

Having identified the modes that must be retained in order to predict correctly the local branching behavior we next construct the minimal system. We set[4]

$$\psi = \mathrm{Re}\left(\frac{2\sqrt{2p}}{ik} e^{ikx}\sin(\pi z)\, a_{11}(t') - \frac{p}{\pi ik}\sin(2\pi z)\, a_{02}(t') + \frac{2\sqrt{2p}}{ik} e^{ikx}\sin(3\pi z)\, a_{13}(t') \right), \tag{11a}$$

$$\theta = \mathrm{Re}\left(2\sqrt{\frac{2}{p}}\, e^{ikx}\sin(\pi z)\, b_{11}(t') - \frac{1}{\pi}\sin(2\pi z)\, b_{02}(t') + 2\sqrt{\frac{2}{p}}\, e^{ikx}\sin(3\pi z)\, b_{13}(t') \right), \tag{11b}$$

$$\Sigma = \mathrm{Re}\left(2\sqrt{\frac{2}{p}}\, e^{ikx}\sin(\pi z)\, d_{11}(t') - \frac{1}{\pi}\sin(2\pi z)\, d_{02}(t') + 2\sqrt{\frac{2}{p}}\, e^{ikx}\sin(3\pi z)\, d_{13}(t') \right), \tag{11c}$$

TABLE I. Modes retained in the spatial Fourier expansion of Eqs. (1).

Order	ψ	θ	Σ
ε	$e^{ikx}\sin(\pi z)$	$e^{ikx}\sin(\pi z)$	$e^{ikx}\sin(\pi z)$
ε^2		$\sin(2\pi z)$	$\sin(2\pi z)$
ε^3	$e^{ikx}\sin(3\pi z)$	$e^{ikx}\sin(3\pi z)$	$e^{ikx}\sin(3\pi z)$
ε^4	$\sin(2\pi z)$		

where $t' = pt$. Substituting into Eqs. (1), and equating terms of like spatial structure we obtain the following set of equations:

$$a'_{11} + (\varpi - 1)a_{11}a_{02} + (\varpi + 1)a_{13}a_{02} = \sigma(rb_{11} + Srd_{11} - a_{11}) , \quad (12a)$$

$$a'_{02} - \varpi(a_{11}a^*_{13} - a^*_{11}a_{13}) = -\sigma\varpi a_{02} , \quad (12b)$$

$$a'_{13} + \left(\frac{1-\varpi}{1+2\varpi}\right) a_{11}a_{02} = \frac{\sigma}{1+2\varpi}(rb_{13} + rSd_{13}) - \sigma(1+2\varpi)a_{13} , \quad (12c)$$

$$b'_{11} + a_{11}b_{02} - b_{11}a_{02} - a_{13}b_{02} + b_{13}a_{02} = a_{11} - b_{11} , \quad (12d)$$

$$b'_{02} - \tfrac{1}{2}\varpi(a_{11}b^*_{11} + a^*_{11}b_{11} - b_{11}a^*_{13} - b^*_{11}a_{13} - a^*_{11}b_{13} - a_{11}b^*_{13}) = -\varpi b_{02} , \quad (12e)$$

$$b'_{13} - a_{11}b_{02} + b_{11}a_{02} = a_{13} - (1+2\varpi)b_{13} , \quad (12f)$$

$$d'_{11} + a_{11}d_{02} - d_{11}a_{02} - a_{13}d_{02} + d_{13}a_{02} = a_{11} - \tau d_{11} + \tau b_{11} , \quad (12g)$$

$$d'_{02} - \tfrac{1}{2}\varpi(a_{11}d^*_{11} + a^*_{11}d_{11} - d_{11}a^*_{13} - d^*_{11}a_{13} - a^*_{11}d_{13} - a_{11}d^*_{13}) = -\varpi\tau d_{02} + \varpi\tau b_{02} , \quad (12h)$$

$$d'_{13} - a_{11}d_{02} + d_{11}a_{02} = a_{13} - (1+2\varpi)\tau d_{13} + (1+2\varpi)\tau b_{13}, \quad (12i)$$

where the prime denotes differentiation with respect to t', and $r \equiv R/R_0$. These equations constitute the required minimal system.

The appearance of the complex amplitudes is a consequence of the O(2) symmetry. When all amplitudes are real Eqs. (12) reduce to the corresponding set for the Z_2-symmetric problem. Note that in this system the mode a_{02} vanishes. The Z_2-symmetric system admits stationary solutions corresponding to steady convection (SS) obtained by setting $d/dt' \equiv 0$. In addition, a branch of SW bifurcates from R_{Hopf}. Within the Z_2-symmetric system we can determine the stability of the SS and SW branches with respect to amplitude perturbations. In particular, a zero eigenvalue corresponds to a saddle-node bifurcation and its corresponding eigenvector is real. This analysis follows closely that given by DaCosta, Knobloch, and Weiss[18] for thermosolutal convection. We omit the details. In the O(2)-symmetric system the SS and SW solutions are no longer isolated: there is a circle's worth of each, labeled by a phase which specifies the position of the cell boundary relative to an arbitrary origin. Each solution is neutrally stable with respect to translation. In addition, there are bifurcations from the circle of SS and SW solutions, i.e., from a group orbit. These bifurcations occur when an eigenvalue passes through zero, but its eigenvector remains complex. In the case of bifurcation from the SS branch, such a bifurcation produces a branch of traveling waves; in the case of SW it results in a branch of modulated waves. For more details, see Refs. 4 and 8. Consequently, to determine the stability properties of the SS and SW branches it is necessary to linearize about these solutions within the O(2)-symmetric system (12). Finally, the TW branch is determined by looking for solutions in the form

$$(a_{11}, a_{13}, b_{11}, b_{13}, d_{11}, d_{13}) = e^{i\omega_1 t}\ (\hat{a}_{11}, \hat{a}_{13}, \hat{b}_{11}, \hat{b}_{13}, \hat{d}_{11}, \hat{d}_{13}), \quad (13a)$$

$$(a_{02}, b_{02}, d_{02}) = (\hat{a}_{02}, \hat{b}_{02}, \hat{d}_{02}) , \quad (13b)$$

with the "hatted" quantities time independent. The resulting complex algebraic system is readily solved for the amplitudes and the frequency ω_1 as a function of the reduced Rayleigh number r. The TW can propagate either to the left or the right, and are therefore isolated solutions. They may lose stability at a zero eigenvalue corresponding to a saddle-node bifurcation, or through a Hopf bifurcation which gives rise to a branch of modulated waves. In the remainder of this paper we explore the various interconnections among the solution branches.

In order to guide the exploration we review briefly the results of analyzing the TB bifurcation with O(2) symmetry which occurs at

$$r_c = 1 + \frac{\tau}{\sigma}(1+\tau)(1+\sigma) , \quad (14a)$$

$$S_c = \frac{-\tau^2(1+\sigma)}{\sigma + \tau(1+\tau)(1+\sigma)} . \quad (14b)$$

Near this point Eqs. (12) reduce to an amplitude equation of the form[4,8]

$$\ddot{a}_{11} = (\mu + A|a_{11}|^2)a_{11} + \varepsilon[\ \nu\dot{a}_{11} + C(a_{11}\dot{a}^*_{11} + a^*_{11}\dot{a}_{11})a_{11} + D|a_{11}|^2\dot{a}_{11}] + O(\varepsilon^2), \quad (15)$$

where μ and ν are linearly related to $(r - r_c)/\varepsilon^2$ and $(S - S_c)/\varepsilon^2$ and the dot denotes differentiation with respect to the slow time $\varepsilon t'$. Here $A \propto -R_2^{\text{SS}}$ and is positive, $D \propto -R_2^{\text{TW}}$ and vanishes, while $2C + D \propto -R_2^{\text{SW}}$ and is negative. Although the fact that D vanishes formally renders the analysis of Ref. 8 inapplicable to the present problem, one may argue (cf. Ref. 4) that it should behave in accordance with the predictions for D small and negative (when $R_4^{\text{TW}} > 0$) or D small and positive (when $R_4^{\text{TW}} < 0$). These predictions are sketched in Fig. 2.

In Fig. 2(a) ($R_4^{\text{TW}} > 0$) the TW branch bifurcates supercritically, and loses stability at a secondary Hopf

bifurcation giving rise to stable MW. The MW branch terminates on the TW branch in a global bifurcation. If we write the solution to (15) in the form $a_{11} = \mathcal{A}e^{i\omega_1 t}$, then $\mathcal{A} = \mathcal{A}_0$ (constant) describes a traveling wave, while $\mathcal{A} = \mathcal{A}(t)$, $\omega_1 \neq 0$, describes a modulated wave. In the comoving frame the oscillation $\mathcal{A}(t)$ is a standing wave; as the Rayleigh number increases the modulation amplitude also increases, and its period P approaches infinity according to

$$P \sim -\ln(r_h - r), \tag{16}$$

where r_h is the Rayleigh number at which the global bifurcation takes place. The (unstable) TW branch terminates on the (unstable) SS branch, with the phase speed c approaching zero as[19]

$$c \sim (r^{\mathrm{TW}} - r)^{1/2}. \tag{17}$$

The SW branch is unstable throughout, and terminates on the (unstable) SS branch in a heteroclinic orbit; as this point is approached the period again approaches infinity according to (16). In Fig. 2(b) ($R_4^{\mathrm{TW}} < 0$) both the TW and SW branches are unstable throughout, and no secondary bifurcations to MW occur.

In Sec. III we show that these results describe the dynamics of the system (12) over a wide range of parameter values. In addition, however, the presence of a large amplitude stable SS branch is revealed which is connected to the unstable SS branch via a saddle-node bifurcation.

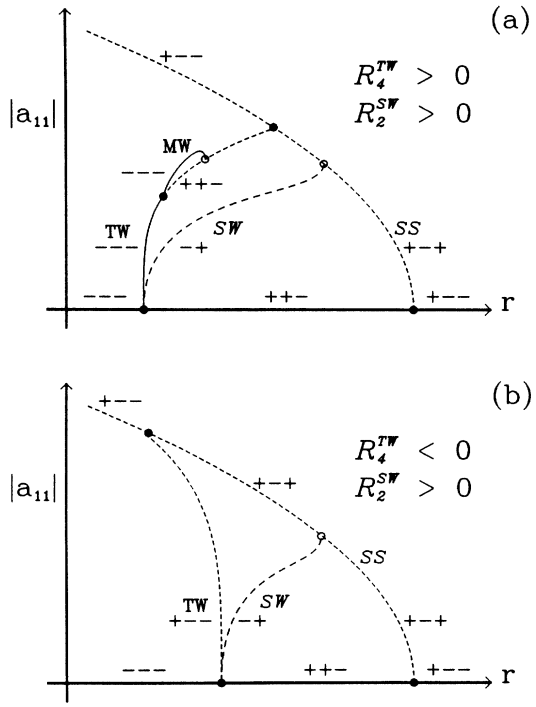

FIG. 2. (a) Schematic bifurcation diagram near a Takens-Bogdanov point with O(2) symmetry when $R_4^{\mathrm{TW}} > 0$ and $R_2^{\mathrm{SW}} > 0$ [region (ii) in Fig. 1(b)]. Stable (unstable) portions of the branches are indicated by solid (dashed) curves. The signs of the principal eigenvalues are shown along each branch. Local bifurcations are marked by solid circles, global bifurcations by open circles. (b) As for Fig. (a) but for region (i) in Fig. 1(b) where $R_4^{\mathrm{TW}} < 0$, $R_2^{\mathrm{SW}} > 0$.

III. THE RESULTS

Equations (12) were solved numerically for steady states and traveling waves. The stability of each solution was determined by numerically solving the appropriate characteristic equation. Owing to the translation symmetry, zero is always an eigenvalue. On the SS branch additional zero eigenvalues occur at a saddle-node bifurcation and at a bifurcation from SS to TW. On the TW branch a zero eigenvalue signals a saddle-node bifurcation, while a Hopf bifurcation gives rise to a secondary MW branch. The SW branch can be found by restricting the variables in Eqs. (12) to be real. This suppresses the instability of SW to TW and enables one to find this branch by solving the time-dependent problem. We have checked our results by expanding each modal amplitude in a Fourier series in time, and obtaining algebraic equations for the amplitudes of the Fourier components. We have found that this method works well for our parameter values provided all the harmonics through fourth order are retained. This yields 12 complex and six real equations for the 30 nonzero coefficients. A similar method was used to construct the MW branch, requiring the solution of 135 simultaneous algebraic equations. This approximation works well provided the modulation is not too nonlinear. Figures 3(a) (inset) and 3(e) indicate the limitations of this method for MW and SW, respectively. In the present problem the MW branch is stable, and so can also be located by direct integration of Eqs. (12). In particular, numerical integration can be used to study the termination of the MW branch, where the algebraic method fails. The integration was carried out using an eighth-order Runge-Kutta scheme[20] with 128-bit precision to ensure adequate accuracy near the end points of the various branches. The algebraic method can also be used to determine the eigenvalues describing the stability of the various branches. In particular, for the TW branch given by (13) essentially exact eigenvalues are readily obtained.

A. Bifurcation diagrams

In Fig. 3(a) we show the bifurcation diagram, $|a_{11}|$ versus r, for parameters characteristic of a ^{3}He-^{4}He mixture: $\tau = 0.03$, $\sigma = 0.6$, $S = -0.01$. Here the TW branch bifurcates supercritically, but loses stability to an MW branch at $r^{\mathrm{MW}} \simeq 1.087\,775$ before terminating on the lower part of the SS branch at r^{TW} ($> r^{\mathrm{MW}}$). Owing to the small range in which the MW branch exists an enlargement of the appropriate portion of the diagram is included. For a slightly lower value of $S, S_{\mathrm{SN}} \simeq -0.012\,500\,6$, the TW branch terminates at the saddle-node (SN) bifurcation on the SS branch, as shown in Fig. 3(b). When $S < S_{\mathrm{SN}}$ the TW branch

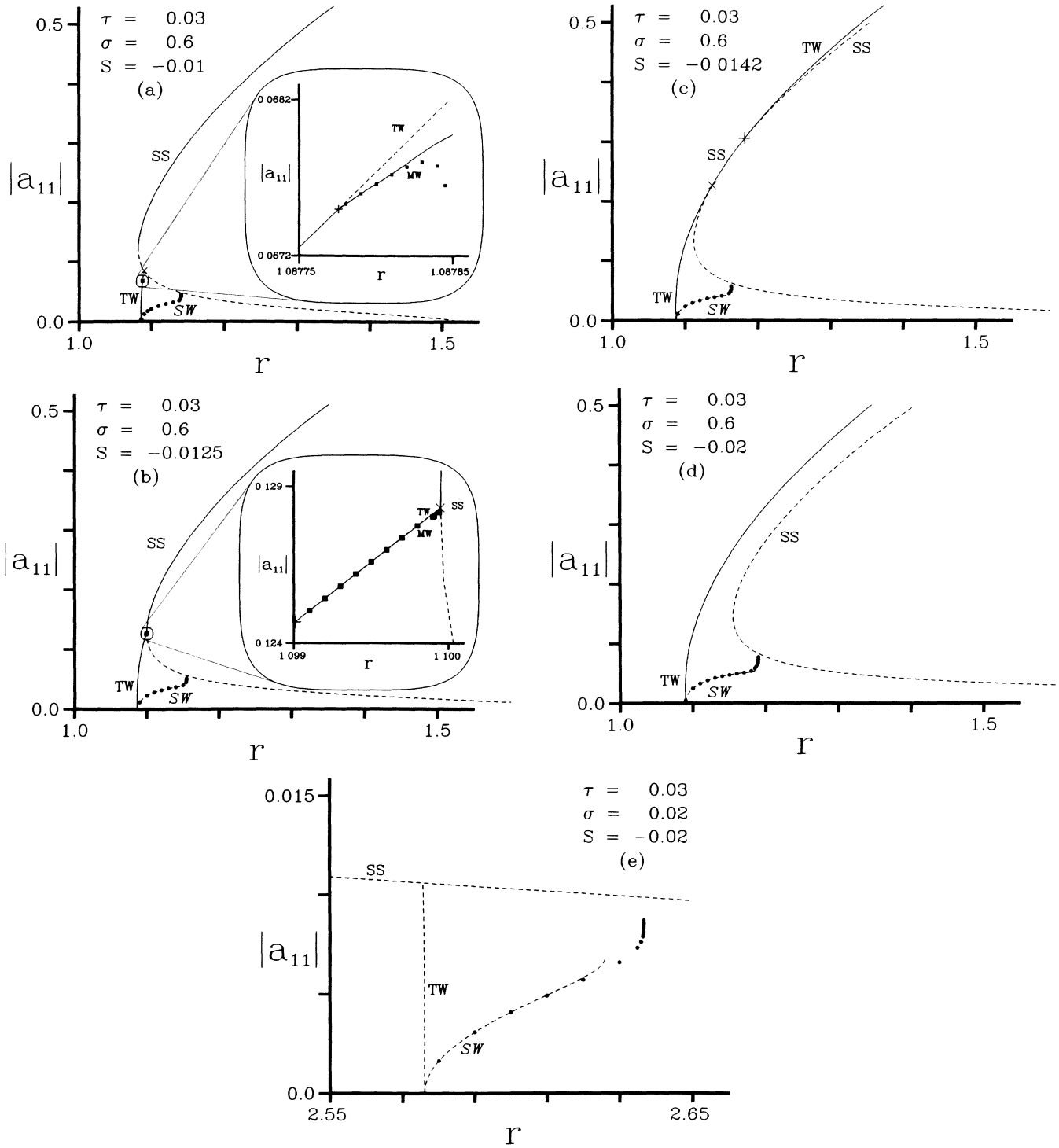

FIG. 3. (a) Bifurcation diagram obtained from Eqs. (12) for parameters appropriate to a ^{3}He-^{4}He mixture, $\tau = 0.03$, $\sigma = 0.6$, and $S = -0.01$. The continuous curves are obtained from the solutions of the algebraic equations appropriate for each branch, the solid curves indicating stable solutions and dashed curves unstable solutions. The circles are numerical values from the integration of Eqs. (12) when all variables are constrained to be real. The squares are values from the integration of Eqs. (12) when complex values are permitted. Both sets of values are square roots of time averages of $|a_{11}|^2$. The inset shows an enlargement of a portion of the $(r, |a_{11}|)$ plane where the TW solutions are unstable to MW. The + marks the Hopf bifurcation of the MW branch from the TW solution, while × marks the termination of the TW branch on the SS branch. (b) As for (a), but with $S = -0.0125$, close to $S_{SN} \simeq -0.012\,500\,6$ where the TW branch terminates at the saddle node on the SS branch. (c) As for (a) and (b), but for $S = -0.0142$. Here the MW are absent and + marks the start of the second TW branch. (d) As for (a)–(c) but for $S = -0.02$. The TW branch never touches the SS branch which remains unstable throughout its upper part. (e) As for (a)–(d) but in region (i) of Fig. 1(b) where $R_4^{TW} < 0$ and the TW branch bifurcates subcritically. In all five cases the SW branch bifurcates supercritically and is unstable throughout.

terminates on the upper part of the SS branch as shown in Fig. 3(c) for $S = -0.0142$. Here the SS branch remains unstable past the saddle node, gaining stability only for $r > r_1^{TW}$. The SS branch remains stable for $r_1^{TW} < r < r_2^{TW}$, but at $r = r_2^{TW}$ it once again loses stability to traveling waves when the dominant eigenvalue returns to the positive half plane. This large amplitude TW branch extends to infinity. Similar behavior was observed in Ref. 11. The values of r_2^{TW} are too large to show the second TW branch in Figs. 3(a) and 3(b), but have been found numerically. For $S < S_d \simeq -0.0143$, the TW branch becomes disconnected from the SS branch which is now unstable for all r. This case is illustrated in Fig. 3(d) for $\tau = 0.03$, $\sigma = 0.6$, $S = -0.02$. At such amplitudes, however, the concentration field will be confined to thin boundary layers and we expect the physical system to behave like pure Rayleigh-Bénard convection. Consequently the stable *large* amplitude TW are likely to be an artifact of the truncation. Finally in Fig. 3(e) we show a case in which the TW branch bifurcates subcritically ($\tau = 0.03$, $\sigma = 0.02$, $S = -0.02$). Note that Figs. 3(a) and 3(e) agree qualitatively with the predictions of the Takens-Bogdanov analysis [Figs. 2(a) and 2(b)].

Observe that in Fig. 3(a) we have a hysteretic transition to steady convection while in Fig. 3(c) the transition is nonhysteretic. In addition, the secondary bifurcation from TW to MW occurs only for $S > S_{SN}$. The value of S_{SN} is readily determined from the requirement that the stability of the SS branch possesses *three* zero eigenvalues at the turning point: one from the translation invariance, the second because it is a saddle-node bifurcation, and the third to allow the TW to terminate there. As S decreases towards S_{SN} the Hopf frequency at the bifurcation from TW to MW decreases to zero so that the TW branch terminates with a double zero eigenvalue, in addition to the third zero from translation invariance. The motion of the relevant pair of eigenvalues along the TW branch as a function of r is shown in Fig. 4 for (a) $S > S_{SN}$, (b) $S \simeq S_{SN}$, and (c) $S < S_{SN}$. Figure 4(a) shows that these eigenvalues are initially real and stable. With increasing r they coalesce on the negative real axis and move into the complex plane. The TW solution undergoes a Hopf bifurcation to MW when these eigenvalues enter the right half of the complex plane. As r increases further the eigenvalues merge onto the positive real axis and then split into two positive real eigenvalues. One of these continues to increase with increasing r while the other decreases, reaching the origin when the TW branch terminates on the SS branch. For $S < S_{SN}$ [Fig. 4(c)] the eigenvalues coalesce on the negative real axis, and the larger real eigenvalue reaches the origin at the end of the TW branch. Consequently, here the TW branch remains stable throughout. At $S = S_{SN}, r = r_{SN}$ [Fig. 4(b)] we have a multiple steady-state bifurcation from a group orbit of nontrivial steady states (see Appendix). The above sequence of transitions is discussed further in Sec. IV. The same conclusions apply if S is held fixed and σ is varied, and allows one to define $\sigma_{SN}(\tau, S)$. Such a

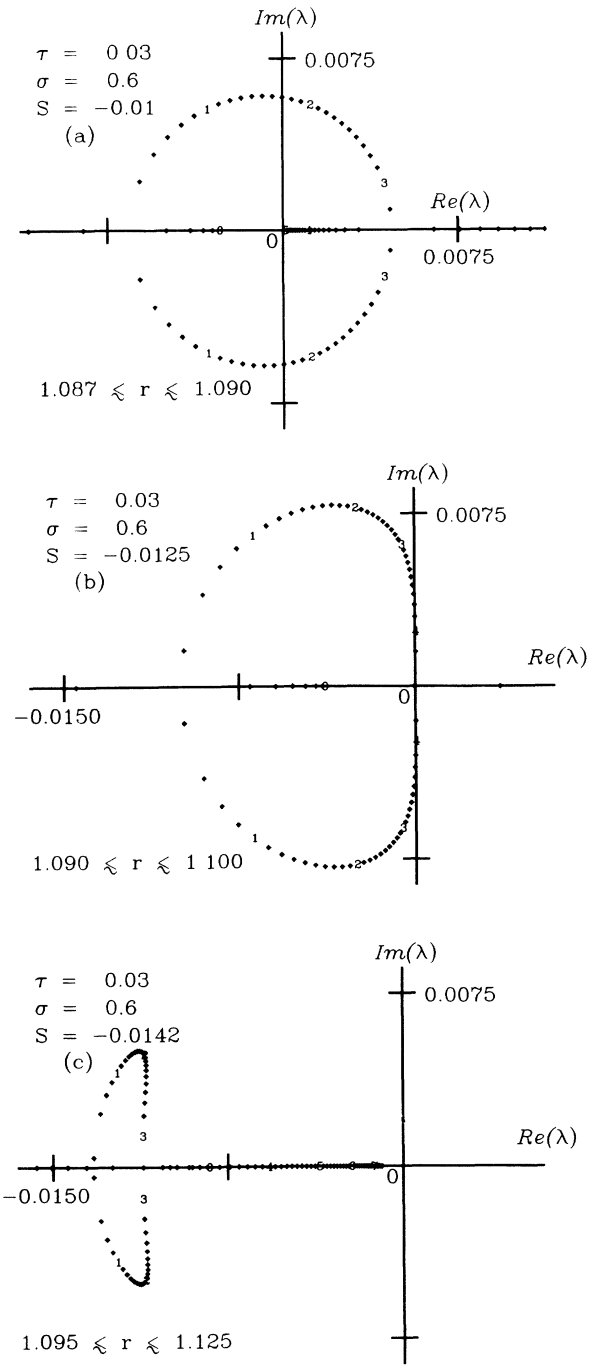

FIG. 4. The motion of the principal eigenvalues along the TW branch as a function of r for $\tau = 0.03$, $\sigma = 0.6$, and (a) $S = -0.01$, (b) $S = -0.0125 \simeq S_{SN}$, (c) $S = -0.0142$. The location of the eigenvalue is shown at a sequence of r values within the interval specified with every tenth point labeled by an integer to indicate the direction of motion with increasing r. In (a) a bifurcation to MW occurs when a pair of complex eigenvalues crosses into the right half plane, and the TW branch terminates when the smaller eigenvalue reaches the origin. In (c) the TW branch remains stable, and terminates when the larger eigenvalue reaches the origin. When $S = S_{SN}$ the TW branch terminates at the saddle node on the SS branch.

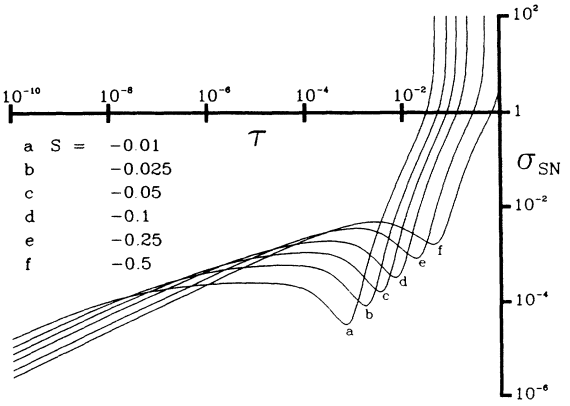

FIG. 5. The quantity $\sigma_{SN}(\tau)$ for several values of S, suggesting that $\sigma_{SN}(0+) \simeq 0.1726(-\tau/S)^{1/2}$, regardless of the value of S.

procedure has an advantage since the SS branch (though not its stability properties) remains unchanged when σ varies. In Fig. 5 we show σ_{SN} as a function of τ for several representative values of S. The figure shows that as τ vanishes $\sigma_{SN} \to \alpha(-\tau/S)^{1/2}$, where $\alpha \simeq 0.1726$. It may be possible to explain this observation using the ideas of Ref. 21, although this is not attempted here.

In Fig. 6 we partition the (σ, r) plane into regimes where stable TW, MW, and SS solutions are located, for the parameter values $\tau = 0.03$, $S = -0.01$. The line labeled Hopf indicates the initial instability of the conduction solution. Since $R_4^{TW} > 0$ stable traveling waves are located to its right. For $\sigma > \sigma_d$ these remain stable for all $r > r_{Hopf}$ [cf. Fig. 3(d)]. For $\sigma_d > \sigma > \sigma_{SN}$ [Fig. 3(c)] the TW branch terminates on the upper SS branch at r_1^{TW} where the SS branch gains stability before losing it again at r_2^{TW} where the large amplitude TW branch bifurcates from

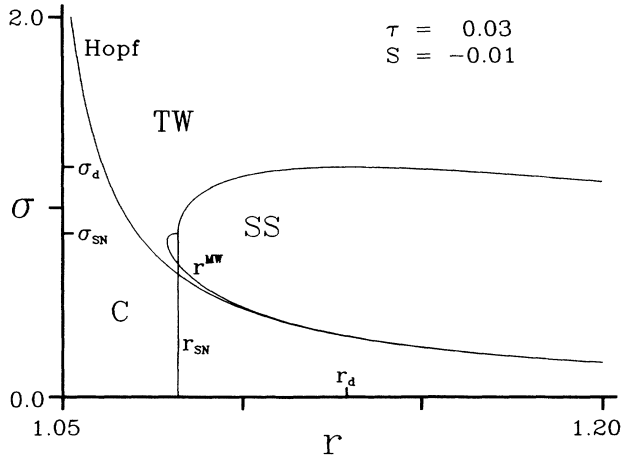

FIG. 6. The (σ, τ) plane for $\tau = 0.03$, $S = -0.01$. The labels C, SS, and TW indicate the location of stable pure conduction, stable steady convection, and stable traveling waves, respectively. Stable modulated waves are found in a narrow region (not indicated) to the right of the line r^{MW}.

it. Consequently the SS solutions are stable only in the range $r_1^{TW} < r < r_2^{TW}$. For $\sigma < \sigma_{SN}$ the SS branch acquires stability at the secondary saddle-node bifurcation. The location of this bifurcation is independent of σ, as indicated by the line $r = r_{SN}$. For $\sigma < \sigma_{SN}$ stable SS are found for $r > r_{SN}$. Finally, the line r^{MW} indicates the Hopf bifurcation to MW from the TW branch. Since this bifurcation is supercritical, stable MW are found for $r > r^{MW}$, but in a region that is too narrow to be visible in the figure. Note that the condition $R_4^{TW} > 0$, necessary for the existence of the MW branch, fails for small σ. This point ($R_4^{TW} = 0$) and the Takens-Bogdanov point are both off scale to the right along the Hopf curve.

In Fig. 7(a) we show the variation of the phase velocity $c \equiv \omega_1/k$, near the end of the TW branch, showing a behavior in excellent agreement with the result (17) fitted to the first two points. In Fig. 7(b) we show the variation of the modulation period P along the MW branch. This period is equal to the period of the mode b_{02} which is proportional to the Nusselt number, and is easily determined since in a modulated wave b_{02} has a

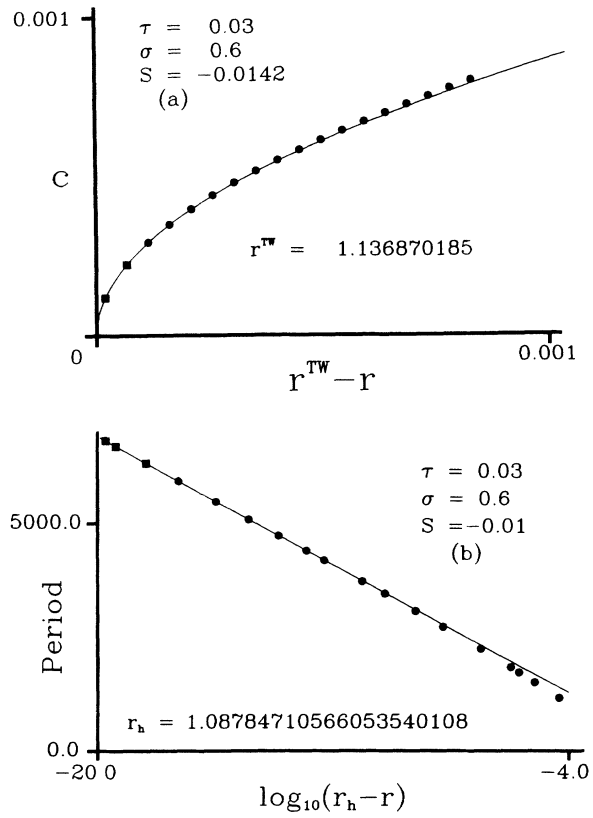

FIG. 7. (a) The phase velocity $c(r)$ near the end of the TW branch for $\tau = 0.03$, $\sigma = 0.6$, $S = -0.0142$. The solid line is a fit of the prediction (17) through the two points denoted by squares showing that $r^{TW} \simeq 1.136\ 870\ 185$. (b) The modulation period $P(r)$ near the end of the MW branch for $\tau = 0.03$, $\sigma = 0.6$, $S = -0.01$. The solid line is a fit of prediction (16) to the three longest periods, denoted by squares, and determines r_h to 20 decimal places.

single frequency ω_2 (and its harmonics) only. The figure shows excellent agreement between the asymptotic relation (16) fitted to the first three points and the remaining points computed numerically, indicating that in the comoving frame the standing wave component of the MW is approaching an infinite period orbit, as suggested by the Takens-Bogdanov analysis. These results provide excellent estimates of the quantities r^{TW} and r_h, i.e., the end points of the TW and MW branches, respectively. We find $r^{TW} = 1.136\ 870\ 185$, while $r_h = 1.087\ 847\ 105\ 660\ 535\ 401\ 08$. As shown below the behavior near r_h is so delicate that accuracy of this magnitude is in fact necessary. These results complete our discussion of the general properties of the bifurcation diagrams, and in particular of the conditions for the presence of an MW branch.

B. Termination of the MW branch

We now turn to more detailed and subtle properties of the modulated traveling waves and discuss the nature of the global bifurcation with which the MW branch terminates. We begin by presenting in Figs. 8(a) and 8(b) the time series for $\mathrm{Re}a_{11}$ at two successive values of r for $\tau = 0.03$, $\sigma = 0.6$, $S = -0.01$ illustrating the rapid lengthening in the modulation period towards the end of the MW branch. The time series for b_{02} corresponding to the series in Fig. 8(b) is shown in Fig. 8(c). Although the time series appears to be complicated owing to the numerous oscillations near the minima it is strictly periodic. For comparison we show in Figs. 9(a) and 9(b) the time series for $\mathrm{Re}a_{11}$ and b_{02} when $\tau = 0.03$, $\sigma = 0.6$, $S = -0.0125$, and $r = 1.099\ 943\ 2$. For this value of S the TW branch terminates just below the saddle-node bifurcation on the SS branch. Although the S values used in Figs. 8 and 9 are quite close, the corresponding time series show marked differences. These can be attributed to the rather different standing wave components of the two waves, as illustrated in Figs. 8(c) and 9(b). Note, however, that a suitable enlargement of the rapid phase of the oscillation shown in Fig. 9(b) reveals a sequence of oscillations near each minimum that is qualitatively similar to the behavior shown in Fig. 8(c). In both sets of figures we indicate also the amplitude of the unstable SS, TW, and SW solutions that coexist with the MW solutions shown. This information will be of vital importance in interpreting the observed structure of the MW.

In Figs. 10(a) and 10(b) these results are presented as limit cycles in the (b_{02}, d_{02}) plane. This projection has the advantage that it removes the oscillation frequency associated with the phase velocity of the traveling wave. Each figure shows the corresponding limit cycles for several values of r showing the approach to the infinite period orbit implied by Fig. 7(b). In this projection the traveling wave appears as a fixed point. Since its position depends on r we indicate by a + its location for the largest r value only. Note, however, that in view of the

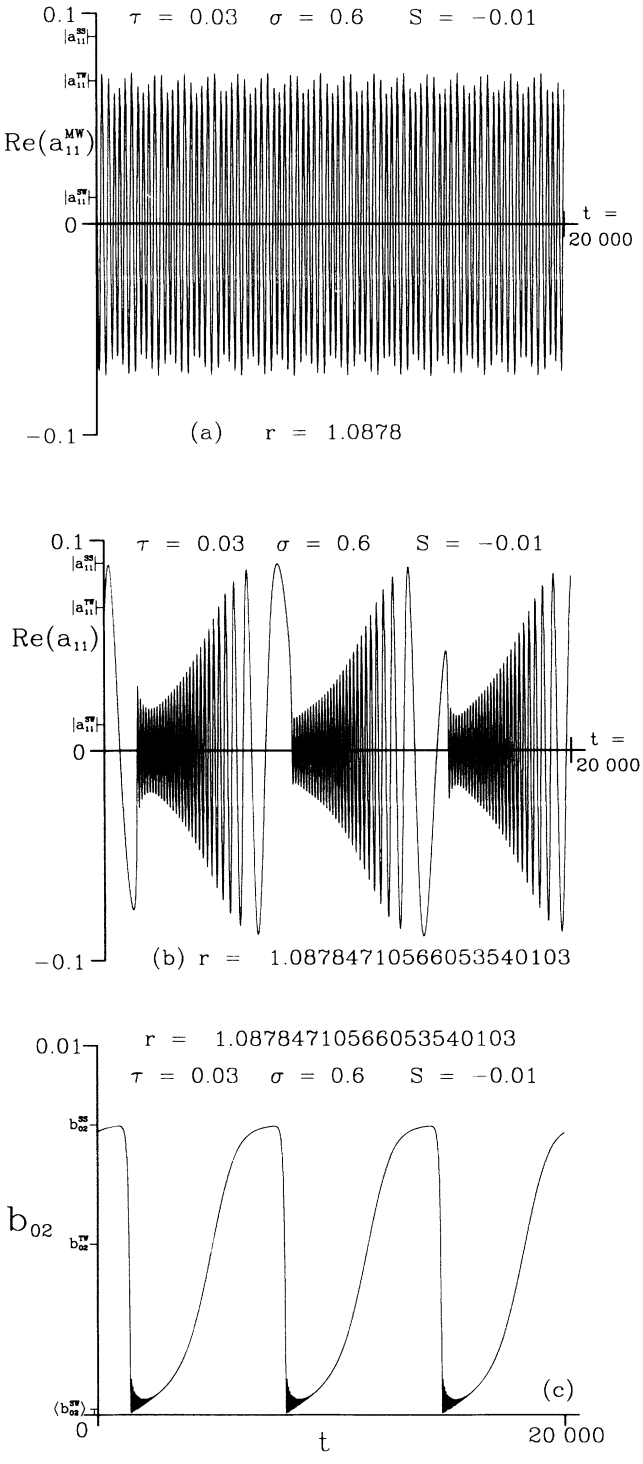

FIG. 8. The time series $\mathrm{Re}a_{11}(t)$ for $\tau = 0.03$, $\sigma = 0.6$, $S = -0.01$ and (a) $r = 1.0878$, (b) $r = 1.087\ 847\ 105\ 660\ 535\ 401\ 03$ showing the rapid increase in the modulation period and amplitude with increasing r. The amplitudes of the coexisting but unstable SS, TW, and SW are labeled using the notation $|\cdots|$. (c) The time series $b_{02}(t)$ corresponding to (b) showing the highly nonlinear standing wave component of the modulated wave. The values of b_{02} for the coexisting SS and TW are indicated, with the notation $<\cdots>$ used to denote the range of oscillation of the coexisting SW.

small increments in r the shift in its position would in any case not be discernible on the scale of the figures. The same applies to the point representing the circle of steady states and denoted by $\times$. We draw attention to the small amplitude oscillations that these limit cycles develop with increasing r. The indicated location and amplitude of the (unstable) SW limit cycle, again for the largest value of r, strongly suggest that this structure is associated with the presence of nearby standing waves. The structure of Fig. 10(a) is shown in a different projection in Fig. 10(c), and again in Fig. 11, where $\mathrm{Im}a_{11}$ is plotted against $\mathrm{Re}d_{11}$ every time $\mathrm{Re}a_{11} = 0$ with $\mathrm{Re}\dot{a}_{11} > 0$. This procedure defines a section through the MW torus by a plane Σ. Figure 11 shows the resulting Poincaré sections for several values of r. Since a MW must take the form $a_{11} = f(\omega_2 t)\exp i\omega_1 t = |f(\omega_2 t)|\exp[i\omega_1 t + i\phi(\omega_2 t)]$, the Poincaré section exhibits points at times satisfying $\omega_1 t + \phi(\omega_2 t) = (2n+1)\pi/2$, n = integer. For a TW the map is therefore a time-T map, where $T = 2\pi/\omega_1$, but for a MW the times between successive points are not equal. Note that the drift frequency ω_1^{MW} for a modulated wave differs in general from ω_1^{TW}, the drift frequency for a

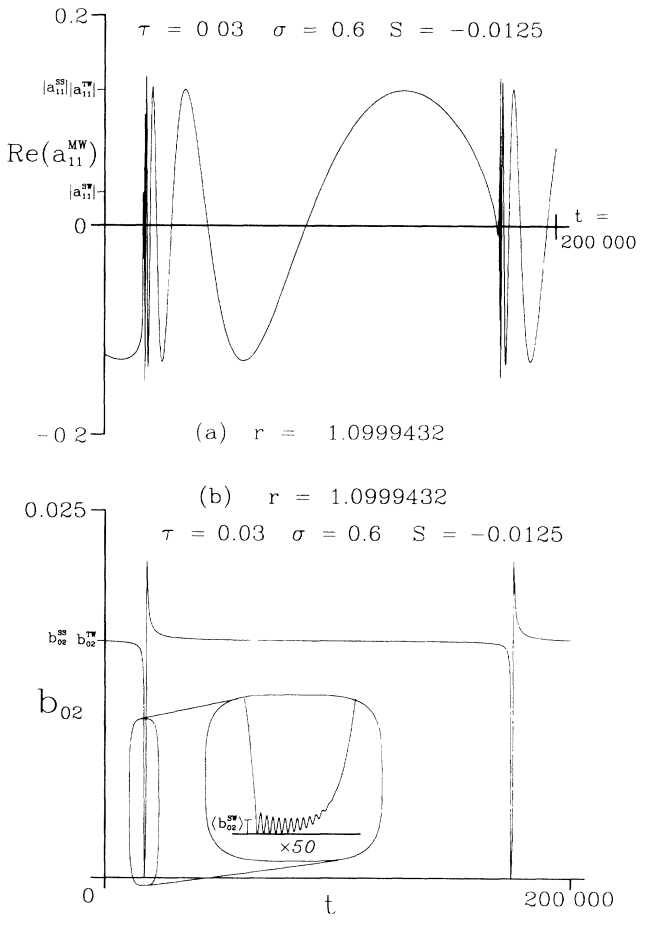

FIG. 9. The time series (a) $\mathrm{Re}a_{11}(t)$, (b) $b_{02}(t)$ for $\tau = 0.03$, $\sigma = 0.6$, $S = -0.0125$, and $r = 1.099\,943\,2$. The inset shows a stretch by a factor of 50 in t near a minimum in the time series (b) showing behavior similar to that of Fig. 8(c).

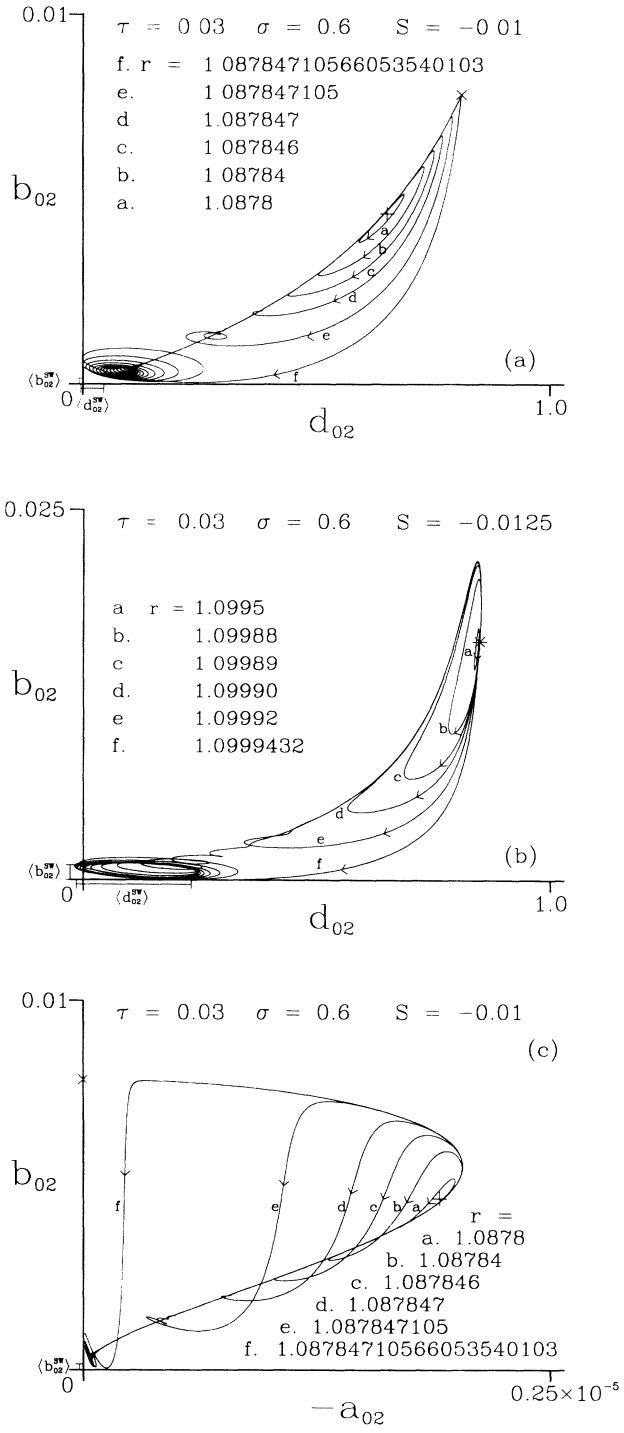

FIG. 10. Limit cycles in the (b_{02}, d_{02}) plane for (a) $\tau = 0.03$, $\sigma = 0.6$, $S = -0.01$, and (b) $\tau = 0.03$, $\sigma = 0.6$, $S = -0.0125$, and several different values of r, showing the rich structure associated with a simultaneous approach to a fixed point representing a steady state and to a limit cycle representing a standing wave. Unstable fixed points corresponding to SS and TW are denoted by $\times$ and $+$, respectively, with the amplitude of the unstable SW limit cycle indicated by $\langle\cdots\rangle$, each for the largest r value shown. (c) As for (a) but showing the $(b_{02}, -a_{02})$ plane.

pure TW at the same value of r, although they agree at r^{MW}. This is because ω_1^{MW} (like ω_2^{MW}) depends on the *amplitude* of the modulation. In Fig. 11 the TW correspond therefore to a fixed point, indicated by +, while the circle of SS is represented by its representative with $\mathrm{Re}a_{11} = 0$ and indicated by ×. Note that such a point necessarily lies on the axis $\mathrm{Re}d_{11} = 0$. Both points are hyperbolic. A pure SW is represented by a limit cycle lying in a plane intersecting the complex a_{11} plane in a straight line through the origin. The limit cycle therefore intersects the plane Σ along the line $\mathrm{Re}a_{11} = \mathrm{Im}a_{11} = 0$; this occurs at a point whose $\mathrm{Re}d_{11}$ coordinate is also indicated in the figure.

We now describe a scenario that accounts for the qualitative aspects of the above results. It is known that sufficiently close to the Takens-Bogdanov bifurcation[8] the MW two-torus does become homoclinic to the TW one-torus as r approaches r_h. In particular, it can be shown that as $r \to r_h$, the drift frequencies ω_1^{MW} and ω_1^{TW} approach one another, and the modulation frequency ω_2^{MW} vanishes. Viewed in the comoving frame the TW fixed point at $r = r_h$ lies *on* the MW limit cycle. Note that this cannot occur in a three-dimensional system since it requires the fixed point to be a generalized saddle, but does occur in the four-dimensional normal form (15) where the TW fixed point has a pair of unstable eigenvalues and a third stable eigenvalue. We remark also that near the Takens-Bogdanov bifurcation ($r_{SS} - r_{Hopf} \ll r_{SS}$) the origin has a pair of unstable eigenvalues of multiplicity two, and hence is repelling in *all* directions. In contrast further away from the Takens-Bogdanov bifurcation the origin acquires a nontrivial stable manifold. For example, in the system (12) this manifold is 11 dimensional and corresponds to real eigenvalues. For case f of Fig. 11 the least stable eigenvalue is $\lambda_3 = -\varpi\tau = -0.08$, while the unstable eigenvalues are $\lambda_1 \pm i\lambda_2$, where $\lambda_1 = 4.089\,92 \times 10^{-4}$ and $\lambda_2 = 5.614\,83 \times 10^{-2}$. Accordingly the MW two-torus *cannot* become homoclinic to the origin near the Takens-Bogdanov bifurcation, but can do so, in principle, further away from it. In fact, the results summarized in Figs. 8(b), 10(a), 10(c), and 13 for $S = -0.1$ indicate that the MW two-torus becomes homoclinic *neither* to the TW fixed point *nor* to the origin (see, in particular, Fig. 12). Figure 10(a) suggests that instead the two-torus is becoming homoclinic to the circle of nontrivial fixed points SS. Each of these is characterized by a phase ϕ and is neutrally stable with respect to changes in ϕ, i.e., spatial translations. Since b_{02}, d_{02} are both real and independent of ϕ this circle appears in Fig. 10(a) as the single point indicated by ×. The development with increasing r of a sharp corner in the limit cycle near this point is characteristic of the approach to a homoclinic orbit. Note that at these parameter values an SS fixed point SS_ϕ has a one-dimensional unstable manifold W_ϕ^u, in addition to a one-dimensional center manifold W_ϕ^c present because of the O(2) symmetry. The unstable manifold lies in a Z_2-invariant subspace, hereafter Σ_ϕ, since it corresponds to an amplitude instability. Since the 13-dimensional stable manifold W_ϕ^s of the fixed point SS_ϕ has a component orthogonal to Σ_ϕ a trajectory in the stable manifold starting with initial conditions that are not reflection invariant (in Σ_ϕ) will result in a drifting state that comes to rest, after an infinite time, at the fixed point SS_ϕ. The trajectory leaves SS_ϕ along its unstable manifold W_ϕ^u,

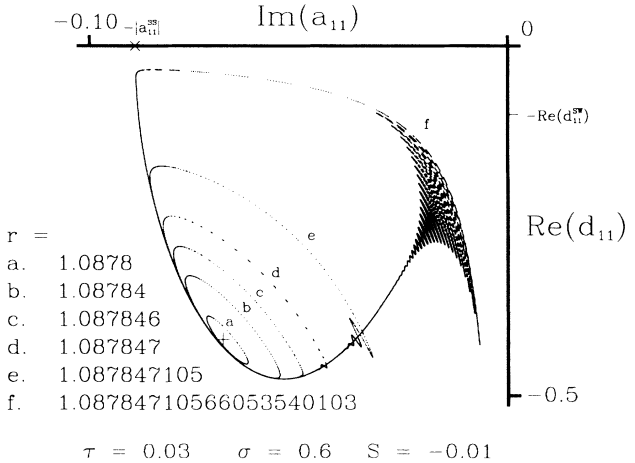

FIG. 11. Poincaré section through the MW two-torus for several values of r corresponding to Fig. 10(a). $\mathrm{Im}a_{11}$ is plotted against $\mathrm{Re}d_{11}$ every time $\mathrm{Re}a_{11} = 0$ with $\mathrm{Re}\dot{a}_{11} > 0$. 100, 500, 500, 1000, 2000, and 40 000 points are plotted to make up sections a through f, respectively. The location of the SS and TW fixed points, and the amplitude of the SW limit cycle are indicated as in Fig. 10, again for the largest value of r.

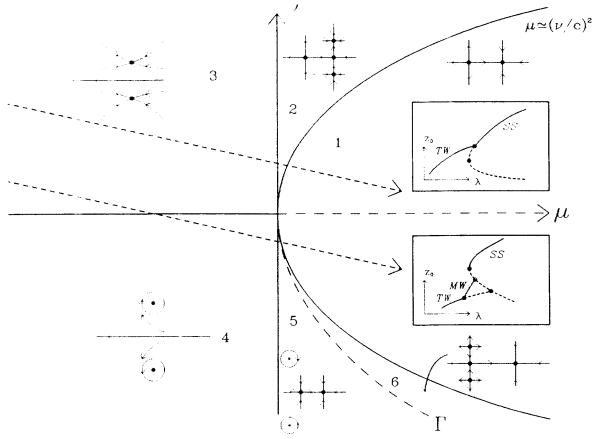

FIG. 12. The (μ, ν) plane for the normal form (18) with $c < 0$, $f < 0$ showing the different phase diagrams $(z(t), y(t))$ characteristic of various regions. The line Γ is a codimension-one surface of global bifurcations. Bifurcation diagrams $z_0(\lambda)$ obtained along typical sections through the (μ, ν) plane are shown as insets. These show stable (unstable) solution branches as solid (dashed) lines, and local (global) bifurcations as solid (open) circles.

approaching the standing waves which are stable in Σ_ϕ. Consequently the trajectory becomes homoclinic to the SW limit cycle with the same phase ϕ, hereafter SW_ϕ, as the fixed point SS_ϕ. This approach to the SW_ϕ limit cycle manifests itself in the fine structure of the oscillations near the origin. Indeed one can verify that the frequency of the oscillations near the origin is close to λ_2 in Fig. 8(b) or $2\lambda_2$ in Fig. 10(a), as appropriate for small amplitude standing waves.[7] Since the SW are unstable with respect to perturbations orthogonal to Σ_ϕ they in turn decay into TW.[3] This instability manifests itself in the decay with time of the oscillations in b_{02}, d_{02}, and a_{02} leaving only those in $a_{11}, b_{11}, \cdots$. Since at these parameter values the TW have a much larger amplitude, the TW amplitude grows exponentially towards the TW fixed point. However, since this point is unstable the solution approaches the MW instead and so drifts again into the circle of fixed points. Thus the MW two-torus becomes heteroclinic to *both* the circle of steady states SS and the circle of standing waves SW. Since ϕ is arbitrary the Z_2-invariant part of the heteroclinic cycle is in fact a circle of heteroclinic orbits. In particular, the phase ϕ of the Z_2-invariant subspace selected by the heteroclinic orbit during the "half" cycle that it spends in such a subspace is undefined. Note that during this "half" of the cycle the resulting MW experiences no drift. This observation illustrates graphically that near $r = r_h$ the MW no longer drifts uniformly (as it does near r^{MW}) but instead drifts in fits and starts. These ideas can also be used to understand the presence of the "fan" that opens out in Fig. 11 with increasing r. Since the SW component of the MW is not a pure SW for any $r < r_h$ the corresponding oscillation in the complex a_{11} plane winds *around* the origin. As a consequence it intersects the plane Σ along a number of points corresponding to different phases of the variable $\mathrm{Re}d_{11}$. The solution therefore samples all values of $\mathrm{Re}d_{11}$ between zero and its value on the circle of steady states. In Fig. 11 the latter is slightly off-scale and describes the maximum vertical extent of the "fan" shown there. Note finally that at r_h both ω_1^{MW} and ω_2^{MW} vanish simultaneously. This does not violate the fact that the two frequencies ω_1^{MW} and ω_2^{MW} cannot lock on the MW two-torus. Indeed it resembles what happens when a two-torus becomes homoclinic to a one-torus with a nonzero frequency ω_1^{TW}. Then, as $r \to r_h$, $\omega_2^{MW} \to 0$ and $\omega_1^{MW} \to \omega_1^{TW}$.

The above scenario is consistent with the available numerical results and argues strongly in favor of the MW two-torus disappearing, for both $S = -0.1$ and $S = -0.125$, by forming a heteroclinic orbit connecting the circle of steady states to the circle of standing waves. This type of heteroclinic orbit has not, to the authors' knowledge, been observed before. Note that in spite of much structure in the two-torus no chaotic behavior was detected. However, any perturbation of the problem that breaks the translation symmetry will result in frequency-locking on the two-torus, and a likely torus breakdown before the dynamics associated with the global bifurcation first appears.[22]

IV. BIFURCATION ANALYSIS NEAR $\sigma = \sigma_{SN}$

Many of the results of the preceding section can be understood simply by constructing a normal form describing the interaction between the TW and SS branches in the vicinity of the saddle-node bifurcation on the latter. This construction is described in the Appendix and leads to the following three-dimensional system:

$$\dot{x} = y \ , \tag{18a}$$

$$\dot{y} = (\nu + cz)y \ , \tag{18b}$$

$$\dot{z} = \mu - z^2 + y^2 + fz^3, \tag{18c}$$

where the variables x and y correspond to position and velocity in the horizontal, and z is an amplitude coordinate relative to the saddle-node amplitude. The parameters μ, ν are unfolding parameters and are linearly related to $r - r_{SN}$ and $\sigma - \sigma_{SN}$. In the normal form (18) we have made a particular choice of signs of the terms y^2, z^2. In the following we show that with this sign choice the signs of c and f can be selected to describe the results of the preceding section. With other choices of signs of y^2, z^2 this is not possible.

Since Eq. (18a) decouples from the other two, the normal form is effectively two dimensional. A partial analysis of the resulting system is given in Ref. 23. There are two types of fixed points (y, z):

$$(0, z_0): \quad z_0 \simeq \pm\sqrt{\mu} \ \text{ for SS} \ , \tag{19}$$

$$(y_0, z_0): \quad y_0 \simeq \pm\sqrt{(\nu/c)^2 - \mu} \ , \quad z_0 = -\nu/c \ \text{ for TW} \ . \tag{20}$$

The identification of these solutions as SS and TW utilizes (18a) to associate a drift with all solutions for which $y \neq 0$. The SS are stable in the z direction (amplitude direction) if $z_0 > 0$, and in the y direction (phase direction) if $\nu + cz_0 < 0$. The saddle-node bifurcation occurs when $\mu = 0$; the bifurcation to TW occurs along $\mu \simeq (\nu/c)^2$. When $c > 0$ the TW fixed points are saddles and undergo no bifurcation. However, when $c < 0$ a Hopf bifurcation occurs along the line

$$\nu = 0, \tag{21}$$

and a stable (unstable) limit cycle forms provided $f < 0$ ($f > 0$). In view of the drift associated with the bifurcating fixed point such limit cycles must be identified with the modulated traveling waves (MW) of Sec. III.

We summarize the results for $c < 0$, $f < 0$ in Fig. 12. The (μ, ν) plane breaks up into six regions with distinct local phase portraits. The resulting bifurcation diagrams, constructed by taking appropriate cuts through the (μ, ν) plane and also shown in Fig. 12, are precisely of the form found numerically in Sec. III A. In particular, for $\sigma < \sigma_{SN}$ (the lower cut) the TW undergo a secondary Hopf bifurcation to MW; the MW are stable throughout and terminate in a global bifurcation on the lower (unstable)

part of the SS branch, followed by the TW. For $\sigma > \sigma_{SN}$ (the upper cut) the TW remain stable throughout, and terminate instead on the upper part of the SS branch. In the former case the transition to SS is hysteretic; in the latter case it is not. In both cases the TW terminate with the square of the phase velocity approaching zero linearly [$y^2 \sim \mu_0 - \mu$, $\mu_0 \equiv (\nu/c)^2$]. Note that the MW disappear precisely when σ passes through σ_{SN}.

It will be observed that the limit cycles in region 5 of Fig. 12 must disappear in the process of crossing into region 1. It is important to discuss this process and the suitability of (18) for its description. As the boundary $\mu \simeq (\nu/c)^2$, $\nu < 0$ (see Fig. 12), is approached the two fixed points representing TW coalesce with the $O(\mu^{1/2})$ fixed point representing SS. By the time this happens the MW limit cycle must have disappeared and this must take place by means of some global bifurcation. Within the normal form (18) the limit cycle *cannot* become homoclinic to the TW fixed point, and so disappears by becoming heteroclinic to the $O(\mu^{1/2})$ and $O(1)$ SS fixed points. The latter fixed point is not, however, a part of the local analysis and was for this reason discarded in (19). Consequently the normal form cannot describe the fate of the limit cycle. In particular, as the MW limit cycle gets closer and closer to the $O(\mu^{1/2})$ SS fixed point it increases in size and the local analysis breaks down. The limit cycle can therefore become homoclinic to *other* invariant sets such as the SW in the system (12) whose existence is not revealed by a local analysis of this type. Thus all that can be deduced from the local analysis near the saddle node is that the limit cycle must disappear in a global bifurcation for $\mu = \mu_c < (\nu/c)^2$, as indicated by the curve Γ in Fig. 12. The inability of a normal form to describe global bifurcations which nonetheless must occur has been observed before.[24]

It is important to observe that it is possible to go further if one returns to the original system for which the normal form (18) is derived. In the Appendix this is the degenerate Takens-Bogdanov normal form. In this system the $O(1)$ SS fixed point does not exist. Since the origin is unstable and the normal form (18) prohibits the formation of a homoclinic orbit through the TW fixed point the MW limit cycle *must* become heteroclinic to the $O(\mu^{1/2})$ SS fixed point and the only $O(1)$ nondrifting state that *is* present, the standing waves SW. Consequently the presence of the heteroclinic orbit described in Sec. III B can be demonstrated *theoretically* near the degenerate TB bifurcation, when the TW branch terminates just below the SS saddle node. In contrast when the TW branch terminates farther from the saddle node the normal form (18) fails and the analysis of Ref. 8 applies instead. In this case the MW limit cycle becomes homoclinic to the TW.

The codimension-two bifurcation that occurs at $S = S_d$ separating Figs. 3(c) and 3(d) can also be understood using similar techniques. In this case the normal form is[25]

$$\dot{x} = y \ , \tag{22a}$$

$$\dot{y} = (\mu^2 + \nu)y - y^2 \ , \tag{22b}$$

with the case $S > S_d$ ($S < S_d$) corresponding to $\nu < 0$ ($\nu > 0$).

V. DISCUSSION AND CONCLUSIONS

In this paper we have studied the properties of a minimal system describing two-dimensional Boussinesq convection in a binary fluid mixture heated from below. This system was constructed so as to be asymptotically exact at small amplitudes. Our results are summarized in the bifurcation diagrams shown in Figs. 3. We see that in all cases the observed behavior at small to moderate amplitudes agrees with the predictions of the Takens-Bogdanov bifurcation with O(2) symmetry [cf. Figs. 2(a) and 2(b)]. In particular, this applies to the secondary MW branch which bifurcates supercritically and terminates in a global bifurcation. The only difference between the theory of the Takens-Bogdanov bifurcation[4,8] and our numerical results at moderate amplitudes is that the MW two-torus terminates in a heteroclinic bifurcation involving the SS and SW circles instead of the TW one-torus. Consequently we expect a transition with decreasing S from a homoclinic bifurcation involving the TW one-torus to a heteroclinic one involving the SS and SW circles. At a critical value of S there should therefore be a heteroclinic bifurcation at which the MW two-torus becomes simultaneously homoclinic to three invariant sets: TW, SS, and SW. From Figs. 10(a) and 11 it appears that this critical value of S is only slightly larger than -0.1; we have not, however, attempted to locate it. The bifurcation diagrams also reflect the fact that at larger amplitudes the SS branch turns around toward larger Rayleigh numbers; this results in two possible transitions, one hysteretic and the other not, from traveling wave convection to steady overturning convection, as the Rayleigh number increases. These bifurcation diagrams can be obtained from an analysis of a degenerate TB bifurcation with O(2) symmetry as shown in Sec. IV and the Appendix, and qualitatively similar transitions have been observed in experiments in ethanol-water mixtures heated from below.[26] In particular, the vanishing of the TW phase velocity was observed, although the relation (17) could not be verified, perhaps owing to slight hysteresis in the transition arising from small departures from two-dimensional structure in this regime.[26] A related experiment by Heinrichs, Ahlers, and Cannell[27] has revealed a transition from TW to MW whose signature is entirely consistent with the predictions of the TB bifurcation with O(2) symmetry.[28] However, the present model does not predict the correct behavior for ethanol-water mixtures ($\sigma \approx 10$) largely because the TW branch reaches much larger amplitudes than for ^{3}He-^{4}He mixtures ($\sigma \approx 0.6$). In the latter the bifurcation behavior that occurs at small amplitudes, including the MW branch, is believed to be in the range of validity of the model, and hence a property of the partial differential equations for moderate departures from the parameter

values required for the TB bifurcation. A similar correspondence between model solutions and the solutions to the partial differential equations has been established for Z_2-symmetric thermosolutal convection in Ref. 7 and O(2)-symmetric thermosolutal convection in Ref. 29. It should be noted that with identical boundary conditions at the top and bottom finite amplitude TW have, in the comoving frame, the symmetry $(x,z) \to (x+\pi/k, 1-z)$, $(\psi,\theta,\Sigma) \to (-\psi,-\theta,-\Sigma)$. This symmetry allows the centers of neighboring cells to be displaced in opposite directions with respect to the layer midplane.[29,30] These displacements increase from zero with increasing amplitude and are allowed because the reflection symmetry Z_2 takes a traveling wave into a *distinct* state, namely a wave traveling in the opposite direction. In contrast for stationary rolls Z_2 takes a roll solution into minus itself, and hence forces the existence of a solution with cell centers in the midplane. Note that it is the Z_2 symmetry rather than reflection in the midplane that is important here. Although the displacements in a TW of the cell centers are not represented in Eqs. (11), a quantitative comparison for thermosolutal convection between the minimal model and solutions of the partial differential equations shows that the modes retained in (11) consistently contain the most power.[29]

In addition to exploring the bifurcation diagrams away from the codimension-two point, the study of the minimal system has revealed several results of theoretical interest. In particular we have presented evidence that away from the Takens-Bogdanov point the MW branch continues to terminate in a global bifurcation [cf. Fig. 7(b)], albeit of a novel type. This bifurcation is heteroclinic involving the states SS and SW instead of TW, and required extreme accuracy to establish its existence. Of interest also is the observation that modulated traveling waves are present only for $\sigma < \sigma_{SN}$, where σ_{SN} denotes the value of the Prandtl number for which the TW branch terminates at the saddle node on the steady state branch. We found that this behavior could be readily explained by a normal form constructed at the codimension-two point $\sigma = \sigma_{SN}, r = r_{SN}$. The analysis showed that the Hopf bifurcation to MW moves towards the end of the TW branch as the codimension-two point is approached, with the modulation frequency approaching zero. This suggests that in experiments like that of Ref. 26 MW could be realized by increasing S to bring the termination point of the TW branch below the saddle node on the SS branch. We emphasize, however, that this is not the only way for the MW to disappear. For example, farther from the Takens-Bogdanov bifurcation the TW branch may develop a cusp and acquire a loop in which exactly the right number of eigenvalues lose stability for the branch to terminate on the unstable SS branch without a prior bifurcation to MW.[31] We have also seen that for $\sigma < \sigma_{SN}$ the TW branch has two distinct parts, the small amplitude branch from which the MW branch bifurcates, and a large amplitude branch which bifurcates from the upper part of the SS branch. For $\sigma_{SN} < \sigma < \sigma_d$ both TW branches bifurcate from the upper SS branch, and for $\sigma > \sigma_d$ these branches join and detach from the SS branch. Here stable TW exist for all values of the Rayleigh number greater than R_{Hopf}. This property of the model occurs, however, for amplitudes beyond its regime of validity.

The present model is a considerable improvement over the model proposed in Ref. 32. The latter includes only the modes $a_{11}, b_{11}, b_{02}, d_{11}, d_{02}$, with the result that the TW branch is completely degenerate: it exists at $R = R_{Hopf}$ only, a property that could be anticipated from the well-known result that with the present boundary conditions, $R_2^{TW} \equiv 0$.[9] In the minimal system this degeneracy is removed by the higher-order modes, and allows us to study the properties of the secondary MW branch. In addition, the fourth-order calculation required to construct the model revealed the existence of an Eulerian mean flow associated with a traveling wave whose significance for the transport properties of such waves will be discussed elsewhere.[16]

ACKNOWLEDGMENTS

We are very grateful to Professor M. Golubitsky and Professor N.O. Weiss for helpful suggestions and discussions. In particular, the interpretation of the numerical results of Sec. III B owes a great deal to the latter's insight. The work of E.K. was supported in part by the National Science Foundation and the U.S. Defense Advanced Research Projects Agency under Grant No. DMS-8814702. D.R.M. received support from the Institute for Naval Oceanography, which is sponsored by the U.S. Navy and administered by the Office of the Chief of Naval Research.

APPENDIX: DERIVATION OF THE NORMAL FORM (18)

As mentioned in Sec. IV the numerical results may be understood in terms of a codimension-three bifurcation which arises when one of the nondegeneracy conditions in the generic Takens-Bogdanov bifurcation fails. Since the numerical results that are of interest involve interaction between the TW branch and the saddle-node bifurcation on the SS branch, we are interested in unfolding the degeneracy $A = 0$ in the analysis of Dangelmayr and Knobloch.[8] In this appendix we derive the appropriate normal form. However, instead of providing a complete analysis of this normal form, we use it to derive a normal form describing the interaction of the TW and SS branches only, in the case where the latter is close to a saddle-node bifurcation.

As in Ref. 8 we use complex coordinates $(v,w) \in C^2$ and demand that the resulting equations are equivariant under the following representation of the group O(2):

$$R_\theta(v,w) = (e^{i\theta}v, e^{i\theta}w), \quad \text{translations} \tag{A1a}$$

$$\kappa(v,w) = (\overline{v},\overline{w}), \quad \text{reflections} . \tag{A1b}$$

There are three invariants of this action:

$$\sigma_1 = |v|^2, \quad \sigma_2 = |w|^2, \quad \sigma_3 = v\overline{w} + \overline{v}w. \tag{A2}$$

The most general equivariant vector field then takes the form[8]

$$\dot{v} = g_1 v + g_2 w \ , \tag{A3a}$$

$$\dot{w} = g_3 v + g_4 w, \tag{A3b}$$

where $g_j \equiv g_j(\sigma_1, \sigma_2, \sigma_3)$, $j = 1, 2, 3, 4$, are smooth real-valued functions. The Takens-Bogdanov singularity is characterized by the linearization

$$\begin{pmatrix} \dot{v} \\ \dot{w} \end{pmatrix} = \begin{pmatrix} 0 & 1 \\ 0 & 0 \end{pmatrix} \begin{pmatrix} v \\ w \end{pmatrix} \tag{A4}$$

of (A3). Nonlinear near-identity coordinate changes may be carried out to remove as many of the nonlinear terms in (A3) as possible. Omitting the details, we find that at third order in (v, w) four terms remain, while at fifth order there are six terms that cannot be removed:

$$\dot{v} = w + O(7) \ , \tag{A5a}$$

$$\begin{aligned} \dot{w} = {} & B|w|^2 v + C(v\overline{w} + \overline{v}w)v + D|v|^2 w + E|v|^4 v \\ & + F|v|^2|w|^2 v + G|v|^4 w + H|v|^2|w|^2 w \\ & + I|v|^2(v\overline{w} + \overline{v}w)v + J|v|^2(v\overline{w} + \overline{v}w)w + O(7), \end{aligned} \tag{A5b}$$

where $O(7)$ denotes seventh-order terms. In obtaining this normal form we have set the coefficient A of $|v|^2 v$ in (A5b) equal to zero. The resulting degeneracy has codimension-three, and requires three parameters to unfold it. Omitting all higher-order terms, we have

$$\dot{v} = w \ , \tag{A6a}$$

$$\begin{aligned} \dot{w} = {} & \mu v + \nu w + \eta|v|^2 v + B|w|^2 v + C(v\overline{w} + \overline{v}w)v \\ & + D|v|^2 w + E|v|^4 v + F|v|^2|w|^2 v + G|v|^4 w \\ & + H|v|^2|w|^2 w + I|v|^2(v\overline{w} + \overline{v}w)v \\ & + J|v|^2(v\overline{w} + \overline{v}w)w. \end{aligned} \tag{A6b}$$

This is the required truncated normal form. Note that when $\eta = O(1)$ and certain nondegeneracy conditions on the coefficients C and D hold, then the fifth order terms are no longer required and the system (A6) reduces to that analyzed in Ref. 8. In the codimension-three case we treat all three unfolding parameters μ, ν, η as small.

Equations (A6) describe the interaction of TW with the saddle-node bifurcation on the SS branch. By construction it occurs in the neighborhood of the codimension-three singularity, and hence at small amplitude. To obtain equations describing this interaction we introduce real coordinates $v = (x_1, y_1)$, $w = (x_2, y_2)$ in R^4 and choose a particular steady-state solution $(x_1, y_1, x_2, y_2) = (x, 0, 0, 0)$. Because of the O(2) symmetry, rotation through θ generates a nonzero y_1. Thus y_1 represents the coordinate along the group orbit, while the coordinates (x_1, x_2, y_2) are perpendicular to it. By a theorem of Krupa[33] the vector field (A6) may locally be decomposed into a three-dimensional vector field in the perpendicular direction,

$$\dot{x}_1 = x_2 \ , \tag{A7a}$$

$$\begin{aligned} \dot{x}_2 = {} & \mu x_1 + \nu x_2 + \eta x_1^3 + B(x_2^2 + y_2^2)x_1 + M x_1^2 x_2 + E x_1^5 \\ & + F(x_2^2 + y_2^2)x_1^3 + N x_1^4 x_2 + H x_1^2(x_2^2 + y_2^2)x_2 \\ & + 2J x_1^3 x_2^2 \ , \end{aligned} \tag{A7b}$$

$$\dot{y}_2 = [\nu + D x_1^2 + G x_1^4 + H x_1^2(x_2^2 + y_2^2) + 2J x_1^3 x_2]y_2, \tag{A7c}$$

together with a drift along the group orbit:

$$\dot{y}_1 = y_2. \tag{A8}$$

Here $M = 2C + D, N = G + 2I$. Hence to understand the dynamics it is sufficient to analyze (A7).

In the system (A7) the point $(x, 0, 0)$, where

$$\mu + \eta x^2 + E x^4 = 0, \tag{A9}$$

denotes a nontrivial steady state. The point $(x, 0, y)$ represents a traveling wave, where

$$\nu + D x^2 + G x^4 + H x^2 y^2 = 0. \tag{A10}$$

To study the interaction between TW and SS we linearize (A7) about $(x, 0, 0)$. There are three eigenvalues given by

$$\lambda^2 - \lambda(\nu + M x^2 + N x^4) - (\mu + 3\eta x^2 + 5E x^4) = 0 \ , \tag{A11}$$

$$\lambda_3 = \nu + D x^2 + G x^4. \tag{A12}$$

The last eigenvalue describes the bifurcation from SS to TW when it passes through zero. Assuming that both the eigenvalues (A11) have $\mathrm{Re}\lambda \neq 0$, we can carry out a center manifold reduction at $\lambda_3 = 0$, and obtain the normal form

$$\dot{y}_2 = a y_2^3 + O(5) \tag{A13}$$

with an unfolding

$$\dot{y}_2 = \delta y_2 + a y_2^3 + O(5), \tag{A14}$$

where $\delta = O(\lambda_3)$. To Eq. (A14) one must append (A8) describing the drift in the y_1 direction. Thus the fixed point $y_2 = 0$ represents a steady state ($\dot{y}_1 = 0$), but the nontrivial fixed points $\pm y_2$ represent waves traveling in opposite directions ($\dot{y}_1 = \pm y_2$). Consequently (A8) and (A14) establish that, viewed appropriately, the bifurcation to traveling waves is a pitchfork bifurcation.[33] In particular, the usual transfer of stability rules hold for this bifurcation as well.

Of interest is the case when (A11) has a zero eigen-

value, corresponding to a saddle-node bifurcation on the SS branch. The codimension-two bifurcation that arises when this bifurcation interacts with the bifurcation to traveling waves ($\lambda_3 = 0$) will be described by a two-dimensional system. To determine this system we suppose the three eigenvalues (A11) and (A12) are

$$\lambda_1 = \lambda \equiv \nu + Mx^2 + Nx^4, \quad \lambda_2 = \lambda_3 = 0. \tag{A15}$$

Then the linearization of (A7) takes the form

$$\begin{pmatrix} \dot{x}_1 \\ \dot{x}_2 \\ \dot{y}_2 \end{pmatrix} = \begin{pmatrix} 0 & 1 & 0 \\ 0 & \lambda & 0 \\ 0 & 0 & 0 \end{pmatrix} \begin{pmatrix} x_1 \\ x_2 \\ y_2 \end{pmatrix} . \tag{A16}$$

We introduce new coordinates (z_1, z_2) given by

$$z_1 = x_1 - x_2/\lambda \ , \tag{A17a}$$

$$z_2 = x_2/\lambda \ , \tag{A17b}$$

in which (A16) takes the Jordan form

$$\begin{pmatrix} \dot{z}_1 \\ \dot{y}_2 \\ \dot{z}_2 \end{pmatrix} = \begin{pmatrix} 0 & 0 & 0 \\ 0 & 0 & 0 \\ 0 & 0 & \lambda \end{pmatrix} \begin{pmatrix} z_1 \\ y_2 \\ z_2 \end{pmatrix} . \tag{A18}$$

The coordinate z_2 can now be eliminated using center manifold reduction. Omitting the details, we find that on the center manifold

$$z_2 = az_1^2 + by_2^2 + O(3), \tag{A19}$$

with z_1 and y_2 obeying equations of the form

$$\dot{z}_1 = mz_1^2 + ny_2^2 + pz_1^3 + qz_1y_2^2 + O(4) \ , \tag{A20a}$$

$$\dot{y}_2 = (rz_1 + sz_1^2 + uy_2^2)y_2 + O(4). \tag{A20b}$$

Explicit expressions for $a, b, m, \ldots, u$ are readily obtained but will not be necessary in what follows. Equations (A20) may be further simplified by a nonlinear coordinate change of the form[23]

$$z = \alpha z_1 + \gamma z_1^2 + \delta y_2^2 + O(3) \ , \tag{A21a}$$

$$y = \beta y_2 + \varepsilon y_2 z_1 + O(3) \ , \tag{A21b}$$

$$t' = (1 + \eta z_1)^{-1} t. \tag{A21c}$$

Choosing $\alpha, \ldots, \eta$ appropriately one finds that the coefficients m, n can be scaled to ± 1, and three of the four cubic terms eliminated:

$$z' = \pm z^2 \pm y^2 + fz^3 + O(4) \ , \tag{A22a}$$

$$y' = cyz + O(4). \tag{A22b}$$

Here the prime denotes differentiation with respect to t'. To unfold these equations we allow λ_2 and λ_3 to be small but nonzero, introducing linear terms into (A22). The resulting linear terms may be diagonalized by an additional near-identity coordinate change;[34] a small shift in the origin of z yields finally the system

$$z' = \mu \pm z^2 \pm y^2 + fz^3 + O(4) \ , \tag{A23a}$$

$$y' = (\nu + cz)y + O(4). \tag{A23b}$$

Here μ, ν are the two unfolding parameters and are linearly related to λ_2, λ_3. The $O(4)$ terms may be dropped provided the nondegeneracy conditions

$$c(0) \neq 0, \quad f(0) \neq 0 \tag{A24}$$

hold at $\mu = \nu = 0$. This truncated system is the required normal form for the present problem. Together with (A8) it describes the interaction of the TW branch with the saddle node on the SS branch, as discussed in Sec. IV.

Equations (A23) have been studied in two other contexts. They are the normal form for the interaction of a saddle-node bifurcation with a Hopf bifurcation and are analyzed in this context in Ref. 23. They are also the normal form for the interaction of two steady-state bifurcations, one a saddle node and the other a pitchfork.[35] Consequently the existing analysis has merely to be reinterpreted within the present problem (see Sec. IV). Finally it is clear from the above analysis that the normal form equations do not depend in form on the use of the Takens-Bogdanov normal form (A6) which merely allows us to compute the coefficients c and f, as well as the signs of the two quadratic terms, in terms of the various quantities appearing there, and hence in terms of the physical parameters. We do not carry out these computations here, and instead show in Sec. IV that Eqs. (A23) suffice to explain the numerical results, for a suitable choice of coefficients.

---

*Permanent address: Department of Mathematics, Imperial College, London SW7 2BZ, England.

[1] E. Knobloch, A. Deane, and J. Toomre, in *The Physics of Structure Formation: Theory and Simulation*, edited by W. Güttinger and G. Dangelmayr (Springer-Verlag, New York, 1987), pp. 117-129.

[2] D.Ruelle, Arch. Rat. Mech. Anal. **51**, 136 (1973); M. Golubitsky and I. Stewart, Arch. Rat. Mech. **87**, 107 (1985); P. Coullet, S. Fauve, and E. Tirapegui, J. Phys. Lett. (Paris), **46**, L787 (1985).

[3] E. Knobloch, A. Deane, J. Toomre, and D.R. Moore, Contemporary Math. **56**, 203 (1986).

[4] E. Knobloch, Phys. Rev. A **34**, 1538 (1986).

[5] A.E. Deane, E. Knobloch, and J. Toomre, Phys. Rev. A **36**, 2862 (1987).

[6] E. Knobloch and M.R.E. Proctor, J. Fluid Mech. **108**, 291

(1981); H.R. Brand, P. Hohenberg, and V. Steinberg, Phys. Rev. A **30**, 2548 (1984).
[7]D.R. Moore, J. Toomre, E. Knobloch, and N.O. Weiss, Nature (London) **303**, 663 (1983); E. Knobloch, D.R. Moore, J. Toomre, and N.O. Weiss, J. Fluid Mech. **166**, 409 (1986).
[8]G. Dangelmayr and E. Knobloch, Philos. Trans. R. Soc. London Ser. A, **322**, 243 (1987).
[9]E. Knobloch, in *Proceedings of the 1985 Joint ASCE-ASME Mechanics Conference*, edited by N.E. Bixler and E.A. Spiegel (Fluid Eng. Div., ASME, New York, 1985), Vol. 24, p.17.
[10]E. Knobloch, Phys. Fluids **23**, 1918 (1980).
[11]S.J. Linz and M. Lücke, Phys. Rev. A **35**, 3997 (1987).
[12]D.T.J. Hurle and E. Jakeman, J. Fluid Mech. **47**, 667 (1971).
[13]This conclusion is in disagreement with M.G. Velarde and J.C. Antoranz, Phys. Lett. **80**A, 220 (1980).
[14]V.Steinberg and H.R. Brand, Phys. Rev. A **30**, 2366 (1984).
[15]D. Barton and J. Ffitch, Rep. Prog. Phys. **35**, 3, 235 (1972).
[16]E. Knobloch and D.R. Moore (unpublished).
[17]The Eulerian mean flow has been omitted from the model discussed by S. J. Linz, M. Lücke, H. W. Müller, and J. Niederländer, Phys. Rev. A **38**, 5727 (1988).
[18]L. N. Da Costa, E. Knobloch, and N.O. Weiss, J. Fluid Mech. **109**, 25 (1981).
[19]This result is misstated in Refs. 4 and 5; see also J. Greene and J. S. Kim, Physica D **33**, 99 (1988).
[20]E. B. Shanks, Math. Comput. **20**, 21 (1966).
[21]M. R. E. Proctor, J. Fluid Mech. **105**, 507 (1981).
[22]D. G. Aronson, M. A. Chory, G. R. Hall, and R. P. McGehee, Commun. Math. Phys. **83**, 303 (1982).
[23]J. Guckenheimer and P. Holmes, *Nonlinear Oscillations, Dynamical Systems and Bifurcations of Vector Fields* (Springer-Verlag, New York, 1986).
[24]See, for example, J. D. Crawford and E. Knobloch, Physica D **31**, 1 (1988).
[25]M. Golubitsky and D. G. Schaeffer, *Singularity and Groups in Bifurcation Theory* (Springer-Verlag, New York, 1984), Vol. I.
[26]E. Moses and V. Steinberg, Phys. Rev. A **34**, 693 (1986).
[27]R. Heinrichs, G. Ahlers, and D.S. Cannell, Phys. Rev. A **35**, 2761 (1987).
[28]E. Knobloch and J.B. Weiss, Phys. Rev A **36**, 1522 (1987).
[29]A.E. Deane, Ph.D. thesis, University of Colorado, Boulder, 1987; E. Knobloch, A.E. Deane, and J. Toomre, Contemp. Math. **99**, 339 (1989).
[30]W. Barten, M. Lücke, W. Hort, and M. Kamps, Phys. Rev. Lett. **63**, 376 (1989).
[31]D. R. Moore and E. Knobloch (unpublished).
[32]M.C. Cross, Phys. Lett. A **119**, 21 (1986); G. Ahlers and M. Lücke, Phys. Rev. A **35**, 470 (1987).
[33]M. Krupa, Ph.D. thesis, Mathematics Department, University of Houston, Texas, 1988.
[34]J. Guckenheimer and E. Knobloch, Geophys. Astrophys. Fluid Dynamics **23**, 247 (1983).
[35]T. Mullin, K. A. Cliffe, and G. Pfister, Phys. Rev. Lett. **58**, 2212 (1987).